Astronomy & Astrophysics manuscript no. output
November 15, 2024

Constraining the density of HBC^+ in the ISM and DIB correlations at high reddening.

S. Van Schuylenbergh[1] and L. M. M. Rekha[1]

Institute of Astronomy, KU Leuven, Celestijnenlaan 200D, 3001 Leuven, Belgium

Received -; accepted -

ABSTRACT

Context. To investigate the top-down formation theory of carbon fullerenes, the density of HBC^+ is constrained by observing a highly reddened target that shows strong DIBs associated with C_{60}^+. Additionally, DIB correlations are investigated in the high-reddening regime using this new measurement.

Aims. A high-SNR, high-resolution optical spectrum is taken of Cyg OB2 12, a highly reddened B5 star, with the aim of detecting the 2 absorption bands seen in the lab-measured optical spectrum of HBC^+ by Campbell & Maier (2017).

Methods. The target is observed by the high-resolution HERMES spectrometer of the Mercator telescope in four different epochs. Right before and after observing the target, a nearby bright B3 standard star with low reddening is observed. This standard star is used to correct for telluric lines. For the investigation of DIB correlations, a new data-driven method of telluric correction is employed, which does not rely on time-dependent observations of a standard star.

Results. Neither of the DIBs of HBC^+ have been detected. Nevertheless, an upper limit on the column density of HBC^+ in the line of sight towards Cyg OB2 12 could be estimated, resulting in $\sim 3.5 \times 10^{12}$ cm^{-2}, which agrees with, and even improves on the upper limit of 8×10^{12} cm^{-2} estimated by Campbell & Maier (2017). Correlations between the EWs of DIBs and reddening indicate that the EW of the DIBs in the spectrum of Cyg OB2 12 seem to be consistently smaller than what would be expected according to the recent studies.

Key words. Diffuse Interstellar Bands (DIBs) – HBC^+ – ISM: molecules

1. Introduction

Diffuse Interstellar Bands (DIBs) are absorption features seen in optical and infrared spectra, associated with molecules in the ISM. Apart from the two near-IR DIBs associated with singly ionized buckminsterfullerene (C_{60}^+), the carrier molecules of DIBs are not known. The leading hypothesis for the formation of carbon fullerenes is the top-down formation scenario. This explains the formation of the spherical fullerenes from a class of flat hydrocarbon molecules called Polycyclic Aromatic Hydrocarbons (PAHs). These flat molecules consisting of multiple connected benzene rings are thought to curl up into the more stable spherical shape of C_{60}.

This top-down formation hypothesis can be tested by looking for the existence of Polycyclic Aromatic Hydrocarbons in the ISM, in lines of sight where C_{60} has previously been detected. The main challenge in this approach is performing laboratory measurements of the gas-phase optical spectrum of PAHs. Recently, lab data has been published of one such PAH: HBC^+, singly ionized hexa-benzo-coronene (Campbell & Maier 2017). The optical spectrum shows two dominant bands, at 8248 Å and 8281 Å respectively.

The target was chosen from Schlarmann et al. (2021), and simply taken to be the target with the highest column density of C_{60}^+. If the top-down formation hypothesis is assumed to be correct, the density of HBC^+ is expected to be strongly correlated to the density of C_{60}^+. Thus taking the target with the highest column density of C_{60}^+ promises the most chance of detecting HBC^+. As the column density of C_{60}^+ is strongly correlated to the reddening, Cyg OB2 12 is also by far the most reddened target in Schlarmann et al. (2021), with an $E(B-V)$ of 3.31 ± 0.10.

As will be discussed in section 3, no DIB corresponding to HBC^+ could be detected. Nevertheless, these measurements of Cyg OB2 12 are useful to examine DIB correlations in the high-reddening regime, which is the focus of the second part of this research. DIBs showing a tight correlation with reddening can be very useful to estimate the reddening itself, especially if they are strong. For example Munari et al. (2008) have proposed to use the 8620 DIB for this purpose.

However, not all DIBs show a clear correlation with $E(B-V)$, e.g. Li et al. (2019) argue that the column density of Hydrogen – $N(H)$ – should be used to normalize the EW instead of $E(B-V)$ when investigating correlations between DIBs and environmental parameters. Therefore, aside from the correlation between the EW of DIBs and $E(B-V)$, correlations with $N(H)$ and $N(H_2)$ are interesting to investigate. Unfortunately, there are no literature estimates of $N(H)$ or $N(H_2)$ in the line of sight towards Cyg OB2 12, so investigating these correlations in the high reddening regime is not yet possible using these observations.

2. Data and reduction

The target is observed by the high-resolution HERMES spectrometer of the Mercator telescope in four different epochs. Right before and after observing the target, a nearby bright B3 standard star (HD 194335) with low reddening is observed. This standard star is used to correct for telluric lines. Since both dominant absorption bands of HBC^+ (8248 Åand 8281 Å) are in a wavelength range that is heavily contaminated by telluric lines,

a careful method of correcting for these telluric lines is of vital importance.

Typically, before any analysis is done – including the correction for telluric lines – a stellar spectrum is normalised. However, in the case of detecting faint DIBs, performing a global normalisation is unhelpful at best, and counterproductive at worst. Normalising a spectrum, regardless of the method used, typically introduces a systematic error of 1 to a few percent. This is on the same order as the maximum expected depth of the DIBs. Therefore, no normalisation of any kind is done. Instead, the continuum is locally modeled by a straight line during the telluric correction process.

2.1. Telluric Correction – Method A

The motivation of observing a low-reddening standard star as telluric correction instead of using a telluric model is twofold. Most importantly, observing the standard star before and after the target observation allows to measure the telluric lines at the airmass at the start and end of the target observation, provided the exposure time on the standard star is relatively short compared to the exposure time on the target. Secondly, this approach does not introduce any model dependency. One drawback is that exposure time has to be shared across target and standard star, and that the standard spectrum introduces a second source of noise.

The telluric lines are corrected for by dividing the target spectrum $F_{\mathrm{tar}}(\lambda)$ by the spectrum of the standard star. More precisely, a weighted average of the standard spectrum taken before and after the target observation is used. To determine the weight of both spectra, the following telluric 'model' is fitted to a part of the target spectrum:

$$F_{\mathrm{tel}}(\lambda) = (a\lambda + b)\left[(1-\alpha)F_{s,0} + \alpha F_{s,1}\right] \quad (1)$$

The correction spectra observed before and after the target observation are $F_{s,0}$ and $F_{s,1}$ respectively, α is a factor between 0 and 1, and a and b describe the difference in local continuum. This is fitted to a small window in the target spectrum by simple χ^2 minimisation, where α must be constant throughout the target spectrum, but a and b are different for each position in the spectrum.

It should be noted that this method of correcting for telluric lines relies on the assumption that neither the target nor the correction spectrum has stellar spectral lines in the window that is used for fitting. This assumption is not valid for the 8281 Å band of HBC^+, which is located in a region where the target spectrum is dominated by overlapping Paschen lines. It is therefore not possible to probe the 8281 Å band using this approach, which forced this research to discard it and focus on the 8248 Å band, which is in a clean area of the target spectrum.

2.2. Telluric Correction – Method B

The second part of this research focuses on testing statistical properties of DIBs in the high-reddening regime. For this purpose, many different targets must be examined. Many targets discussed in earlier research have been observed with the Mercator telescope, and thus have data available in the Hermes database. However, since the aforementioned telluric correction method relies on the observation of a standard star right before and after each target observation, it cannot be used for these other targets. Therefore, a different method has to be used.

Again a standard star is used. This time, HD 36267 is used, as it has been observed more with Hermes than HD 194335. The procedure is illustrated in figure 2. To start, all observations of the target and the standard star respectively are co-added.

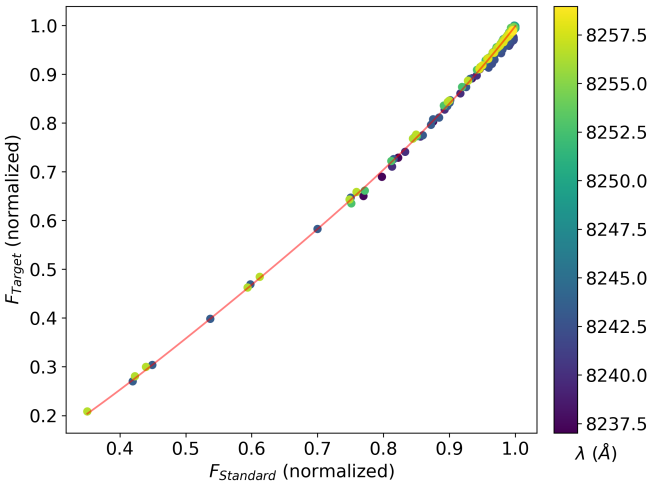

Fig. 1. Mapping of telluric line depth from standard star spectrum to target spectrum.

The Hermes data reduction pipeline automatically shifts a spectrum to correct for the barycentric velocity. This makes sure the spectral features are not red-shifted or blue-shifted due to the orbit of the Earth. As a consequence however, the telluric lines are in a different position for every observation. So before co-adding the spectra, this barycentric velocity correction must be undone, such that the telluric lines are in the same position in each spectrum.

Then both spectra are normalized. Since the standard star is re-used many times, and is used for many different DIBs, it is normalized globally. The target spectrum is normalized locally using a straight line. These normalized spectra are then scaled such that their maximum value between 8237 Å and 8259 Å is unity.

The naive approach to the telluric correction would be to divide the normalized target spectrum by the normalized standard spectrum. However, this does not produce the desired result, as the depth of the telluric lines in the standard spectrum does not match those in the target spectrum. To solve this, a mapping is determined to transform the depth of the telluric lines from the standard spectrum to those in the target spectrum. This mapping is determined by correlating the flux values in the normalized standard spectrum to those in the normalized target spectrum, for wavelengths between 8237 Å and 8259 Å. This is shown in figure 1 for HD 36267 and Cyg OB2 12. This correlation is then fitted by a fourth order polynomial – referred to as the transformation function, f_{trans} – which is shown in red.

By applying this transfer function to each value in the normalized standard spectrum, it is 'transformed' to match the telluric lines of the target spectrum. Dividing the target spectrum by the transformed standard spectrum produces the final spectrum, with telluric lines removed. These last steps are shown in figure 3. The bottom plot shows the (locally) normalized spectrum of Cyg OB2 12 in black, and the transformed normalized spectrum of HD 36267 in red. The middle plot shows a close-up of the same. The final spectrum, obtained by dividing the black spectrum by the red one, is shown in the top plot. As can be seen in figure 3, there is a feature in the target spectrum at 8242 Å, which is not present in the standard spectrum. This feature also shows itself in figure 1, as the blue points slightly below the fit.

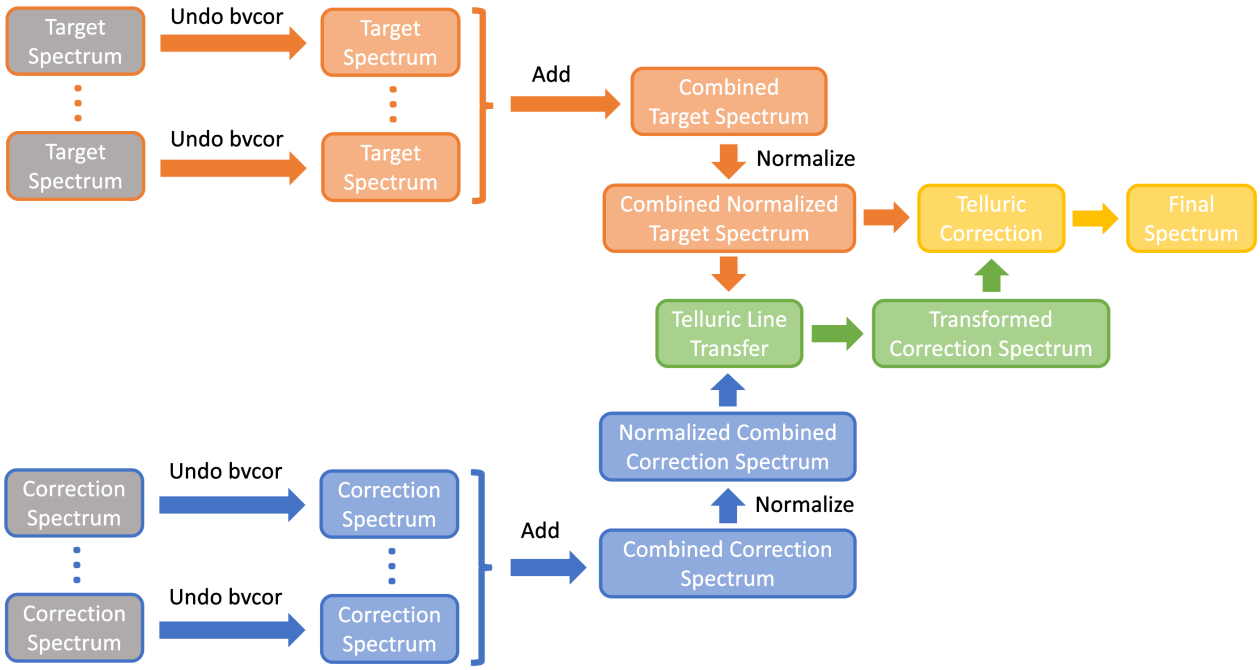

Fig. 2. A flow chart illustrating the procedure of correcting telluric lines with method B.

2.3. Fitting Equivalent Widths

To estimate the EW of a DIB, a model profile is fitted to a small window in the observed spectrum. The model consists of a straight continuum and a line profile of depth ε:

$$F_M = (a\lambda + b)(1 - \varepsilon P(\lambda)) \tag{2}$$

The line profile $P(\lambda)$ can be of any shape, depending on the shape of the DIB. Perhaps the simplest profile is a Gaussian, which is usually a decent approximation for most symmetrical shapes. However, not all DIBs have a symmetrical shape. To model an asymmetrical line profile, a Gaussian profile can be used, with a different σ left and right of the mode. The actual function used for fitting is a re-parameterised variant, with a parameter for the width σ, and the shape s:

$$P(\lambda) = (a\lambda + b)(1 - \varepsilon e^{-x^2/2}) \tag{3}$$

$$x(\lambda) = \frac{\tan\left(\frac{\pi}{2}s\right) + \tan\left(\frac{\pi}{2}(1-s)\right)}{2\sigma}(\lambda - \lambda_0)\begin{cases}\tan\left(\frac{\pi}{2}s\right) & \lambda \le \lambda_0 \\ \tan\left(\frac{\pi}{2}(1-s)\right) & \lambda > \lambda_0\end{cases}$$

This asymmetric profile is only used for fitting when enough evidence is present for an asymmetrical shape. In practice, both profiles are fitted, as well as a model without a line, and their AIC is compared. Only when the AIC of the asymmetrical model is below that of the symmetrical model is the EW calculated from the asymmetric fit. If the AIC of the flat model is lowest, the DIB is considered not detected. In this case, the EW is zero, with an error of the noise level at the position of the DIB.

3. Results

3.1. HBC^+

To investigate the presence of a DIB in the 8248 Å region, the data obtained from the standard star across the four different epochs is combined using the telluric model described in section 2.1. The final spectrum is obtained by dividing each target spectrum by their respective standard spectrum $F_{\rm tel}$ and co-adding those. Using this method, most of the telluric lines in the region of interest are removed and the averaged finalized spectrum is as shown in figure 4. The gray shaded area is the 2σ error margin on the averaged spectrum. In an attempt to boost the SNR, this spectrum is binned per 10 pixels, creating a medium-resolution spectrum of about three times higher SNR. This binned spectrum is depicted in blue. The error estimation for this binned spectrum is computed based on the local variance within each bin.

As can be seen in figure 4, there is no sign of the 8248 Å band of HBC^+. This means that the 8248 Å DIB has a depth of at most the 1-σ error margin. The 1-σ error on the final spectrum is about 0.3%. Using this, an upper limit on the column density of HBC^+ ions along the line of sight towards Cyg OB2 12 can be estimated by

$$N(\mathrm{HBC^+}) = 10^8 \frac{m_e c^2}{\pi e^2} \frac{EW_\lambda}{\lambda^2 f} \tag{4}$$

where m_e is the mass of the electron, c is the speed of light in vacuum, e is the charge on the electron, and f is the oscillator strength, which is taken to be 3×10^{-3} for 8248 Å, as reported by Campbell & Maier (2017). This results in an upper limit for the column density $N(\mathrm{HBC^+})$ of approximately 3.5×10^{12} $\mathrm{cm^{-2}}$. Since Campbell & Maier (2017) do not report a profile or FWHM of the 8248 Å band of HBC^+, it was assumed that the width of DIBs at 8248 Å and 8281 Å are similar. This estimate agrees with, and improves upon, the previously proposed upper limit of 8×10^{12} $\mathrm{cm^{-2}}$ by Campbell & Maier (2017).

3.2. DIB Statistics

Figure 7 shows the relationship between equivalent widths and reddening. The equivalent width measured in this research is

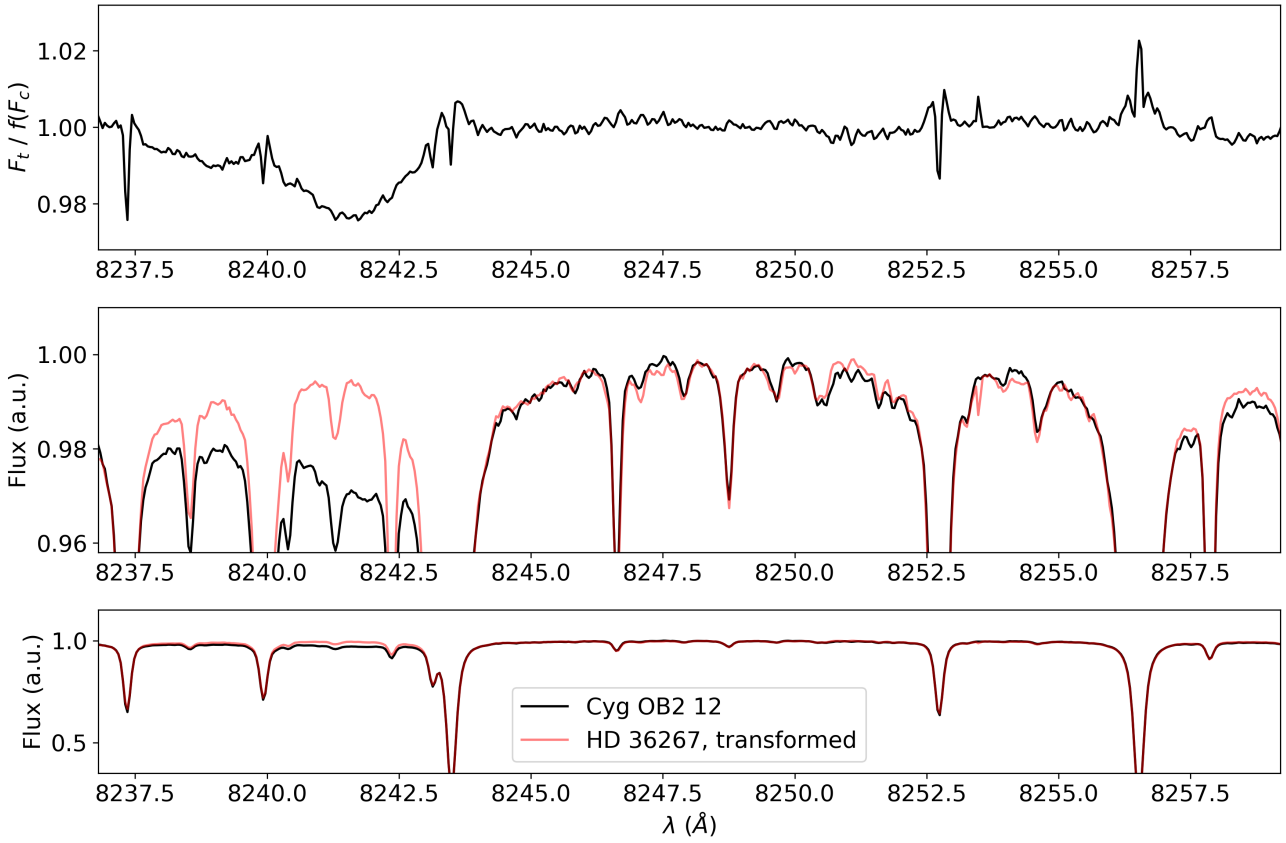

Fig. 3. Final steps in the telluric correction process (method B). The bottom plot shows the (locally) normalized spectrum of Cyg OB2 12 in black, and the transformed normalized spectrum of HD 36267 in red. The middle plot shows a close-up of the same. The final spectrum, obtained by dividing the black spectrum by the red one, is shown in the top plot.

shown in red. In black is shown the EW for different targets from Xiang et al. (2017), Galazutdinov et al. (2008) and Krelowski et al. (1993). The comparison reveals that the EW of DIBs in the spectrum of Cyg OB2 12 seems to consistently fall below the trend established by other observed targets. Such a divergence can be due to a systematic error present in the estimation of the E(B-V) of the target. To verify the value of E(B-V) reported in Schlarmann et al. (2021), the SED of Cyg OB2 12 – obtained from the SIMBAD database Wenger et al. (2000) – is fitted with a Kurucz model, which resulted in an estimate for E(B-V) that agreed with 3.31 ± 0.10.

4. Discussion

4.1. EW Fitting Method

Due to the telluric correction process, target spectra are co-added while each spectrum is slightly shifted due to the barycentric velocity at the epoch of the observation. This means that when the spectra are co-added, all DIBs are in slightly different locations in each of the spectra. This results in a change in shape of the DIBs in the co-added spectrum, complicating the blended profile, as illustrated in figure 5. This can lead to systematic errors.

The extent of the systematic errors caused by this effect have been investigated with a simple synthetic test. For different shapes and widths of a theoretical profile described by equation (3) – using $a = 0$, $b = 1$ and $\varepsilon = 1$ – the following process is done:

1. 10 to 30 barycentric velocity shifts are generated. 5 to 15 from a Gaussian distribution centered on -1 and with $\sigma = 1$, and 5 to 15 from a Gaussian distribution centered on 1 and with $\sigma = 1$.
2. The theoretical profile is taken for every barycentric velocity shift, and the average of all these shifted profiles is taken to create the blended profile. This is shown in the bottom plot of figure 5 in black.
3. This blended profile is then fitted by the theoretical profile, where σ, s and ε are now free parameters, but $a = 0$ and $b = 1$ are still fixed. This is shown in figure 5 in red.
4. Steps 1-3 are done 10,000 times for each combination of shape and width.

The results of these tests are shown in figure 8. For DIBs with σ smaller than or equal to the typical shifts due to the barycentric velocity, the EW is typically overestimated by 1-2%, and the systematic error can be significant compared to the statistical error of the fit. The range of barycentric velocities depends somewhat on the target, but is about -30 to 30 km/s for Cyg OB2 12. This translates into a value for σ of about 0.6 Å, below which these systematic effect are significant. For wider DIBs these effects quickly become negligible. The shape of the profile has little effect on the strength of these systematic effects.

A second test that can be done to verify whether the estimated equivalent widths are reliable, is to compare them to literature values. To do this, 109 targets are taken from Xiang et al. (2017), Galazutdinov et al. (2008) and Krelowski et al. (1993). For these targets, the DIBs that have an EW reported are fitted

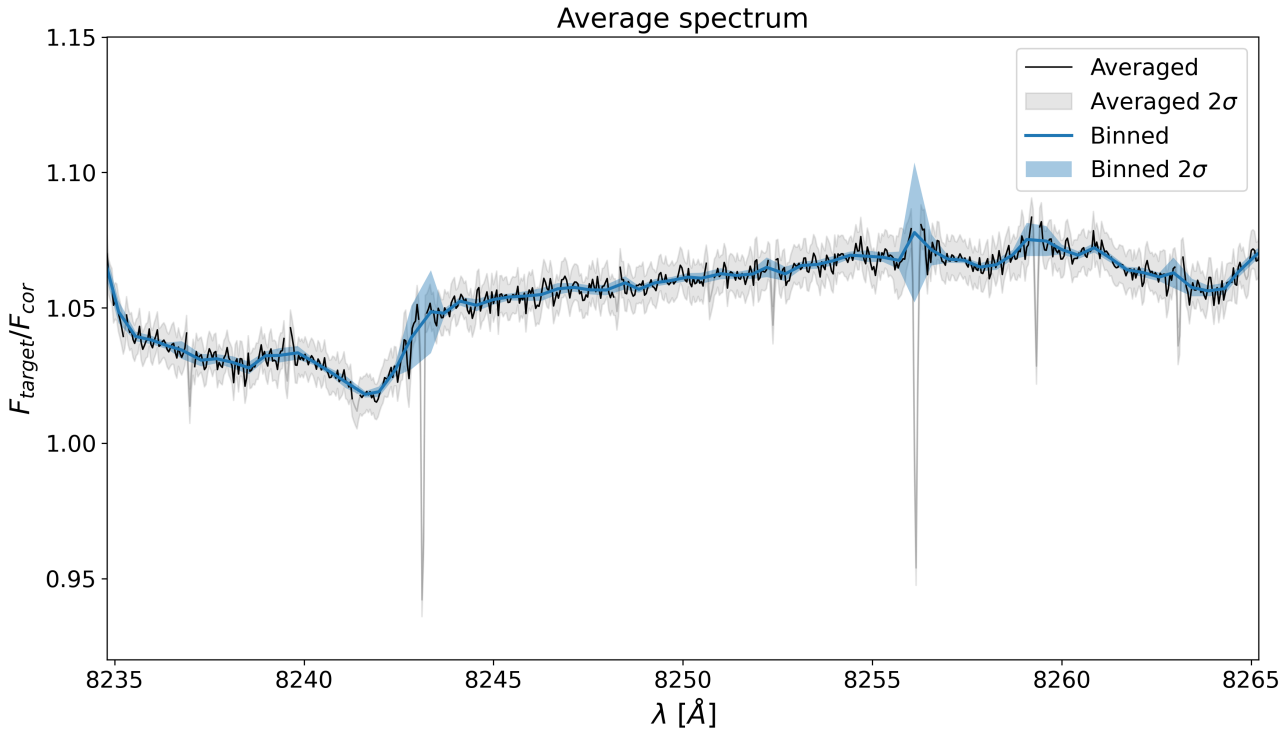

Fig. 4. Averaged spectrum of all four epochs, with telluric lines removed. The gray shaded area shows the 2σ error on the averaged spectrum. In blue is shown a binned spectrum, where the spectrum is binned per 10 data points. The error on this binned spectrum is based on the local variance. Points in the center of telluric lines are excluded from this binning. These excluded points are not drawn in the black line.

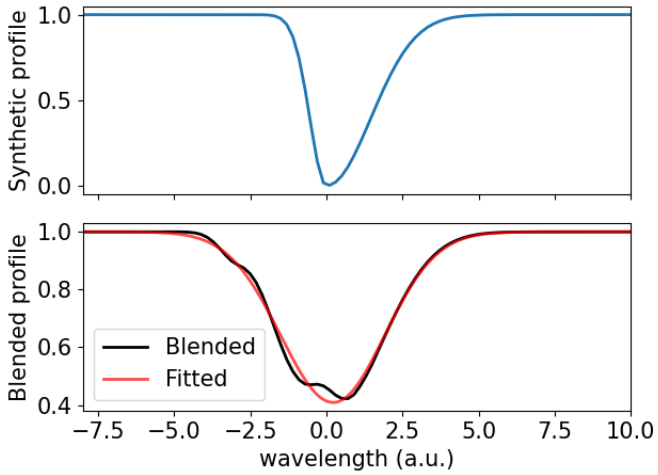

Fig. 5. Effect of co-adding shifted profiles. The resulting blended profile has a complex shape, which is not entirely captured by the function used for fitting. This can result in systematic errors.

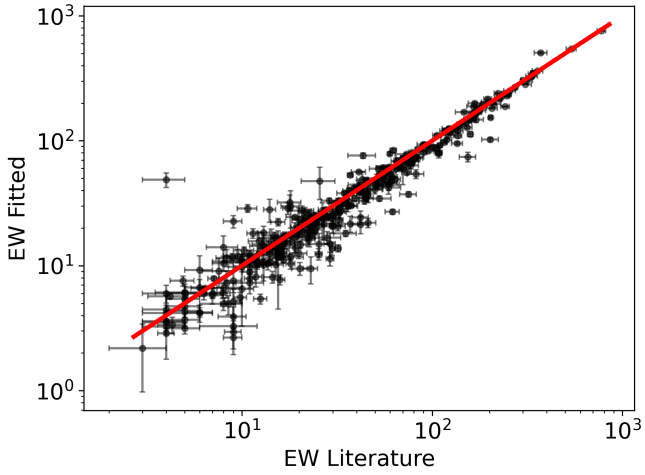

Fig. 6. Comparison of EW fitted with the technique described in section 2.3 and EW reported in Xiang et al. (2017), Galazutdinov et al. (2008) and Krelowski et al. (1993).

using the technique described in section 2.3. These fitted equivalent widths are then compared to the literature value, which is shown in figure 6. A 1-1 correlation is shown in red. In general, the fitted equivalent widths agree well with literature values, with a single exception, which might be attributed to a blend with another DIB or a stellar line.

5. Conclusions

To detect HBC^+, a highly reddened target star Cyg OB2 12 is observed. A standard star (HD 194335) is used to correct for telluric lines. No DIB at 8248 Å could be detected. This allowed to estimate an upper limit on the column density of HBC^+ ions along the line of sight towards Cyg OB2 12. The upper limit on $N(HBC^+)$ is computed to be around $3.5{\times}10^{12}$ cm^{-2}, which aligns with the estimated upper limit of 8×10^{12} cm^{-2} by (Campbell & Maier (2017)).

Even though HBC^+ could not be detected, the data obtained for this study still proved valuable in examining the statistical properties of DIBs in the high-reddening regime. A new data-driven method for telluric correction is employed, which does not rely on time-dependent observations of a standard star. This allowed to co-add all observations of a target in the Hermes database, significantly boosting the SNR.

Equivalent widths of various DIBs were estimated by fitting a symmetric and asymmetric Gaussian profile. The AIC of both of these fits is assessed to decide on the appropriate profile for estimating the EW.

The fitting method is tested for systematic errors and biases in two different ways. A synthetic test showed that the fitted EW can be biased by 1-2% and show systematic errors of $\sigma_{\rm sys} \sim 1\%$ if the DIB is narrow. A second test compared fitted EWs to values found in literature, and showed no significant biases.

Acknowledgements. We are grateful to acknowledge the telescope time on the Mercator telescope granted by Hans Van Winckel and Andrew Tkachenko, as well as their technical support. This research has made use of the SIMBAD database, operated at CDS, Strasbourg, France

References

Campbell, E. K. & Maier, J. P. 2017, ApJ, 850, 69
Galazutdinov, G. A., LoCurto, G., & Krełowski, J. 2008, ApJ, 682, 1076
Krelowski, J., Snow, T. P., Papaj, J., Seab, C. G., & Wszolek, B. 1993, ApJ, 419, 692
Li, K., Li, A., & Xiang, F. Y. 2019, Monthly Notices of the Royal Astronomical Society, 489, 708
Munari, U., Tomasella, L., Fiorucci, M., et al. 2008, A&A, 488, 969
Schlarmann, L., Foing, B., Cami, J., & Fan, H. 2021, A&A, 656, L17
Wenger, M., Ochsenbein, F., Egret, D., et al. 2000, A&AS, 143, 9
Xiang, F. Y., Li, A., & Zhong, J. X. 2017, ApJ, 835, 107

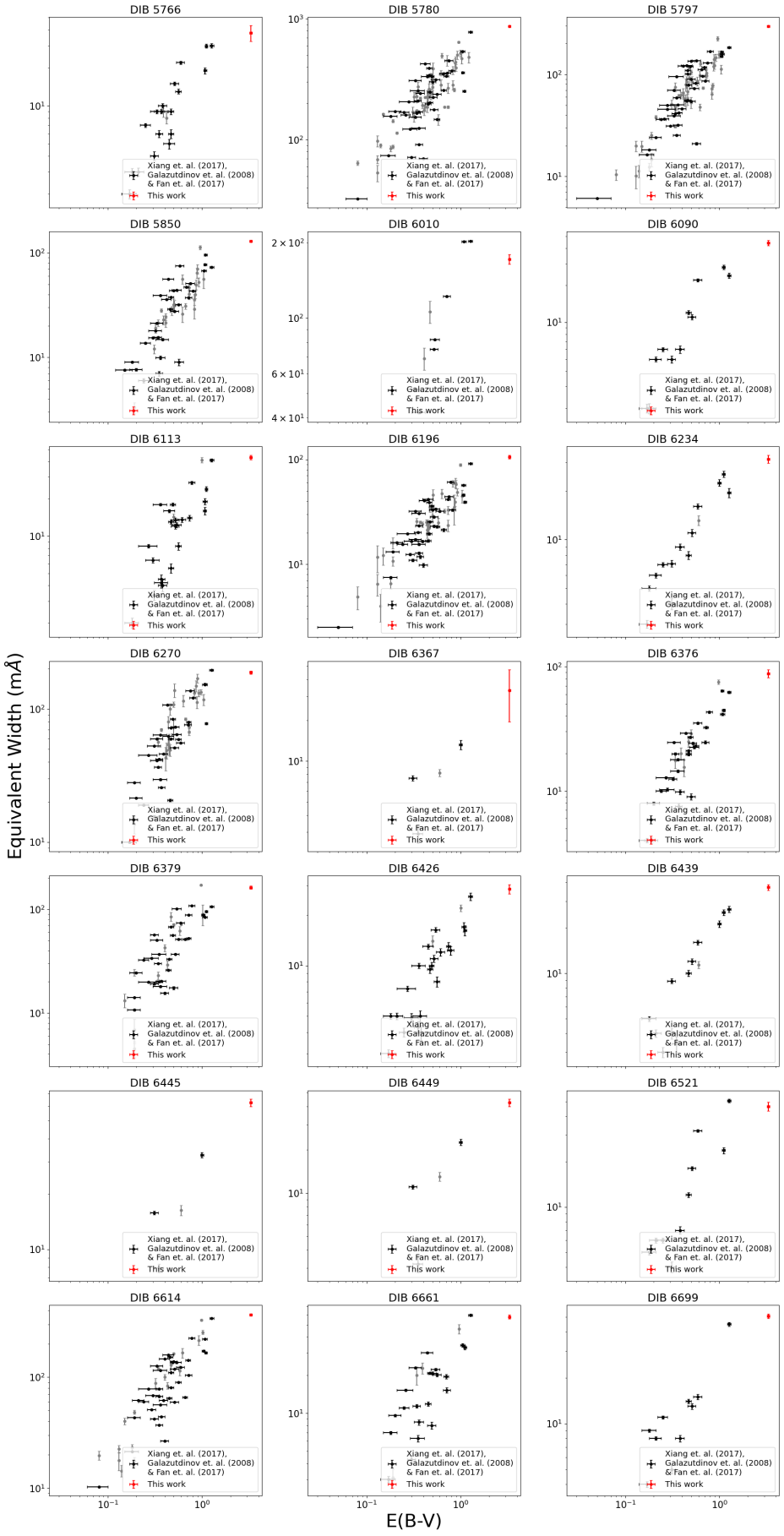

Fig. 7. Correlation between the EW of 21 DIBs and the reddening of the target.

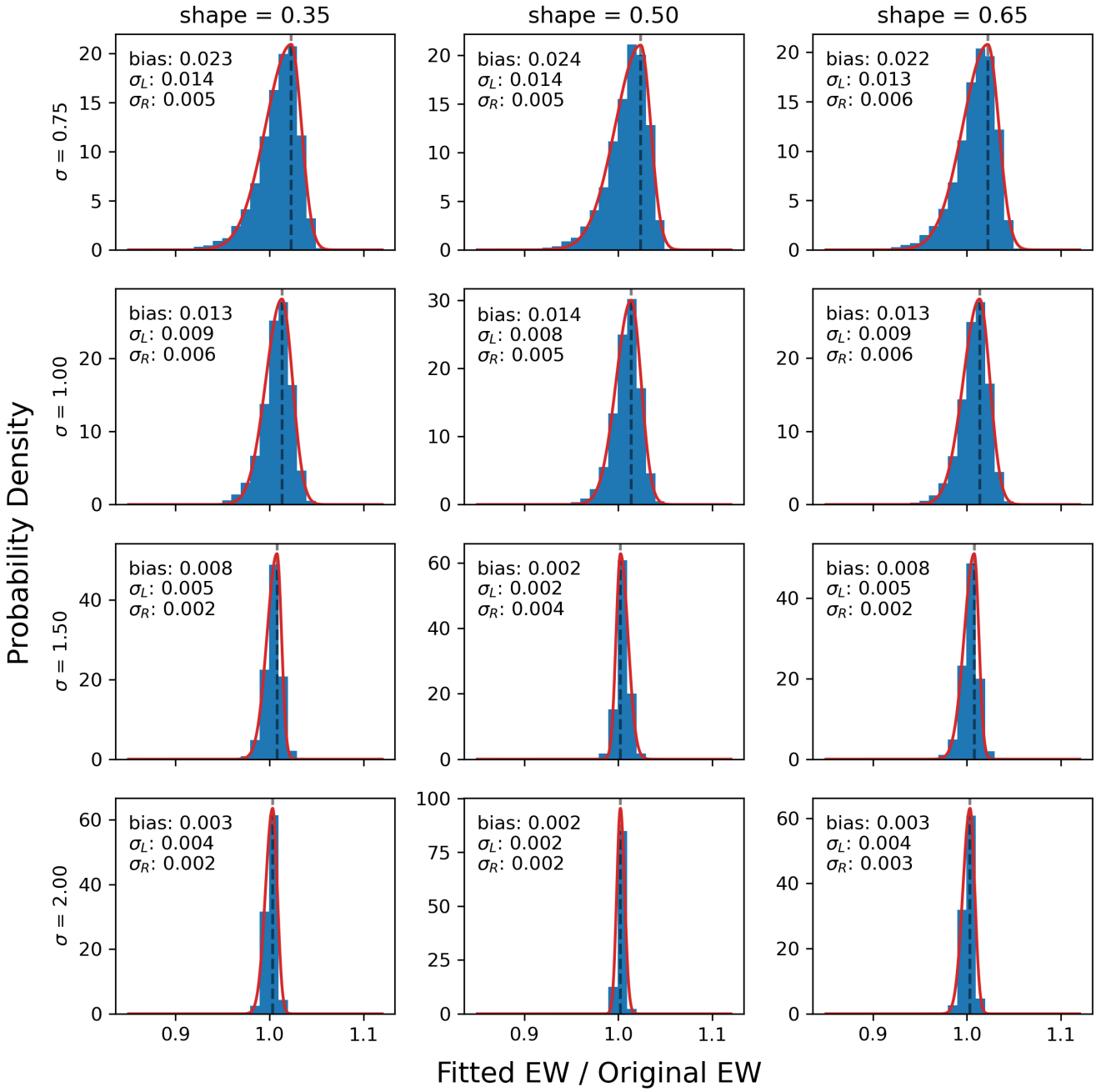

Fig. 8. Biases and systematic errors due to the blending of DIBs as described in section 4.1. For DIBs with widths smaller than or equal to the typical shifts due to the barycentric velocity, the EW is typically overestimated by 1-2%, and the systematic error can be significant compared to the statistical error of the fit. For wider DIBs these effects quickly become negligible. The shape of the profile has little effect on the strength of these systematic effects.